576 *Inorg. Chem.* **2011**, *50*, 576–589
DOI: 10.1021/ic101665g

Inorganic Chemistry
Article

Structure, Properties, and Theoretical Electronic Structure of UCuOP and NpCuOP

Daniel M. Wells,[†,‡] Emilie Ringe,[†] D. Kaczorowski,[§] D. Gnida,[§] G. André,[∥] Richard G. Haire,[⊥] Donald E. Ellis,[†,‡,#] and James A. Ibers*[,†]

[†]*Department of Chemistry, Northwestern University, 2145 Sheridan Road, Evanston, Illinois 60208-3113, United States,* [‡]*Materials Research Center, Northwestern University, 2145 Sheridan Road, Evanston, Illinois 60208-3113, United States,* [§]*Institue of Low Temperature and Structure Research, Polish Academy of Sciences, 50-950 Wroclaw, Poland,* [∥]*Laboratoire Léon Brillouin, CE-Saclay, 91191 Gif sur Yvette Cedex, France,* [⊥]*Chemical Science Division, Oak Ridge National Laboratory, Oak Ridge, Tennessee 37831, United States, and* [#]*Department of Physics & Astronomy, Northwestern University, 2145 Sheridan Road, Evanston, Illinois 60208-3113, United States*

Received August 16, 2010

The compounds UCuOP and NpCuOP have been synthesized and their crystal structures were determined from low-temperature single-crystal X-ray data. These isostructural compounds crystallize with two formula units in space group *P*4/*nmm* of the tetragonal system. Each An atom (An = U or Np) is coordinated to four O and four P atoms in a distorted square antiprism; each Cu atom is coordinated to four P atoms in a distorted tetrahedron. Magnetic susceptibility measurements on crushed single crystals indicate that UCuOP orders antiferromagnetically at 224(2) K. Neutron diffraction experiments at 100 and 228 K show the magnetic structure of UCuOP to be type AFI $(+\,-\,+\,-)$ where ferromagnetically aligned sheets of U atoms in the (001) plane order antiferromagnetically along [001]. The electrical conductivity of UCuOP exhibits metallic character. Its electrical resistivity measured in the ordered region with the current flowing within the tetragonal plane is governed by the scattering of the conduction electrons on antiferromagnetic spin-wave excitations. The electrical resistivity of single-crystalline NpCuOP shows semimetallic character. It is dominated by a pronounced hump at low temperatures, which likely arises owing to long-range magnetic ordering below about 90 K. Density of state analyses using the local spin-density approximation show covalent overlap between AnO and CuP layers of the structure and dominant contributions from 5f-actinide orbitals at the Fermi level. Calculations on a $2 \times 2 \times 2$ supercell of NpCuOP show ferromagnetic ordering within the Np sheets and complex coupling between these planes. Comparisons of the physical properties of these AnCuOP compounds are made with those of the family of related tetragonal uranium phosphide compounds.

Introduction

Studies of the physical and chemical properties of solid-state nonoxide Np analogues of U and Pu compounds are essential for understanding the early actinide elements and their 5f-electrons. These first few elements of the actinide series embody the transition from itinerant to localized 5f-electrons or, in chemical terms, from resembling the transition metals to resembling the rare-earth elements. Whereas the properties of Np binaries are generally intermediate between those of U and Pu, few ternary or quaternary compounds of Np have been synthesized and investigated thoroughly. Knowledge of the structure−function relationship in such Np compounds can lead to enhanced understanding of the early actinide series; comparison of the properties of isostructural compounds can also lead to enhanced understanding of their unique properties.

*To whom correspondence should be addressed. E-mail: ibers@chem.northwestern.edu. Phone: +1 847 491 5449. Fax: +1 847 491 2976.

The quaternary compound UCuOP crystallizes in the space group *P*4/*nmm* of the tetragonal system in the ZrCuSiAs[1] structure-type, the same structure type as the recently reported superconductor LaFeOP.[2] UCuOP was the first synthesized quaternary oxypnictide whose structure was solved by single crystal X-ray diffraction methods[3] and can be considered archetypal to the "1111" superconducting iron arsenide compounds. It shows antiferromagnetic ordering at $T_N = 220(2)$ K and a low-temperature rise in magnetic susceptibility below 80 K.[3] Beyond its interesting structure type and magnetic anomalies, the compound belongs to a class of highly investigated actinide compounds that crystallize in either of two tetragonal space groups, *P*4/*nmm* or *I*4/*mmm*.[4]

(1) Johnson, V.; Jeitschko, W. *J. Solid State Chem.* **1974**, *11*, 161–166.
(2) Kamihara, Y.; Hiramatsu, H.; Hirano, M.; Kawamura, R.; Yanagi, H.; Kamiya, T.; Hosono, H. *J. Am. Chem. Soc.* **2006**, *128*, 10012–10013.
(3) Kaczorowski, D.; Albering, J. H.; Noël, H.; Jeitschko, W. *J. Alloys Compd.* **1994**, *216*, 117–121.
(4) Troc, R. *Inorg. Chim. Acta* **1987**, *140*, 67–77.

 Published on Web 12/15/2010

The U parent compounds UP_2[4−9] and $UCuP_2$[10−13] have been well-studied, whereas the analogous Np/P compounds are unknown. The actinide oxychalcogenides AnOQ[14−18] and pnictide-chalcogenides AnTQ[19−22] (An = U and Np; T = P, As, Sb; Q = S, Se, Te) also belong to this family; they show diverse physical properties. Only the heavier pnictides (T = As, Sb, and Bi) are known to form NpT_2.[23] The properties of cubic NpP and NpAs are similar;[24] one can speculate that the properties of the unknown NpP_2 compound might resemble those of tetragonal $NpAs_2$.[25−31] Np_3P_4 is said to be isostructural to cubic Th_3P_4,[32,33] but the lattice parameter remains unpublished. U and Cu form a second oxyphosphide compound, the quaternary $U_2Cu_2OP_3$[34] (initially characterized as $U_4Cu_4P_7$[35,36]), that can be viewed as a stacking along [001] of structural blocks from UCuOP and $UCuP_2$.[3] A few intermetallic Np/Cu compounds are known[37−41] that are related to superconducting $PuCoGa_5$.[42]

Herein we present the syntheses and properties of UCuOP and the new Np analogue NpCuOP, including crystal structures, electrical resistivities, neutron diffraction and temperature-dependent magnetic susceptibility of UCuOP, and theoretical electronic structures. Concurrent with this work a related study on UCuOP and ThCuOP has appeared.[43]

Experimental Section

Syntheses. Caution! *^{237}Np and any ingrown daughter products are α- and γ-emitting radioisotopes and as such are considered a health risk. Their use requires appropriate infrastructure and personnel trained in the handling of radioactive materials. The procedures we use for the syntheses of Np compounds have been described.*[44] *^{238}U was handled under normal laboratory conditions.*

The following reagents were used as obtained from the manufacturer: Cu (Aldrich, 99.5%), CuO (Aldrich, 99.99%), and P (Aldrich, 99%). Resublimed I_2 available in the laboratory was utilized as a transport reagent. Depleted ^{238}U turnings from Oak Ridge National Laboratory (ORNL) were powdered through three cycles of hydrogenation/dehydrogenation at 573 and 723 K, respectively.[45] The purity of the resultant U powder was confirmed by powder X-ray diffraction methods. ^{237}Np chunks were crushed and used as provided (ORNL).

Synthesis of UCuOP. The original synthesis[3] of UCuOP involved the reaction of UP and CuO, followed by vapor transport with I_2 to afford single crystals. Attempted synthesis of UCuOP using this method was unsuccessful. Here a reaction mixture of 40.0 mg of U powder (0.17 mmol), 8.9 mg of CuO (0.11 mmol), 3.6 mg of Cu (0.056 mmol), and 6.9 mg of P (0.22 mmol) was loaded into a fused-silica ampule in an Ar-filled drybox. The ampule was evacuated to $\sim 10^{-4}$ Torr and flame-sealed. It was then placed in a computer-controlled furnace, heated to 1273 K in 12 h, kept at 1273 K for 96 h, and cooled in three steps, at 5 K/h to 773 K, at 10 K/h to 473, and finally air cooled.

A powder X-ray diffraction pattern of the resultant uniform black powder confirmed the presence of UCuOP. The sample was loaded into a fused-silica ampule with 9.5 mg I_2. It was evacuated to $\sim 10^{-4}$ Torr and sealed. The ampule was placed in a computer-controlled two-zone furnace where a 50 K temperature gradient (1173−1223 K) was held for 120 h. The sample was then cooled to 873 K in 87.5 h, further cooled at 10 K/h to 573 K,

(5) Iandelli, A. *Atti Accad. Naz. Lincei, Cl. Sci. Fis., Mat. Nat., Rend.* **1952**, *13*, 144–151.
(6) Trzebiatowski, W.; Troc, R. *Bull. Acad. Pol. Sci., Ser. Sci. Chim.* **1963**, *11*, 661–664.
(7) Troc, R.; Leciejewicz, J.; Ciszewski, R. *Phys. Status Solidi A* **1966**, *15*, 515–519.
(8) Aoki, D.; Wisniewski, P.; Miyake, K.; Watanabe, N.; Inada, Y.; Settai, R.; Yamamoto, E.; Haga, Y.; Onuki, Y. *Philos. Mag. B* **2000**, *80*, 1517–1544.
(9) Henkie, Z.; Trzebiatowski, W. *Phys. Status Solidi A* **1969**, *35*, 827–834.
(10) Kaczorowski, D.; Troc, R.; Noël, H. *J. Phys.: Condens. Matter* **1991**, *3*, 4959–4970.
(11) Zolnierek, Z.; Kaczorowski, D.; Troc, R. *J. Less-Common Met.* **1986**, *121*, 193–197.
(12) Plackowski, T.; Kaczorowski, D. *Phys. Rev. B* **2005**, *72*, 224407/1–224407/8.
(13) Korner, N.; Schoenes, J.; Kaczorowski, D. *Helv. Phys. Acta* **1989**, *62*, 207–210.
(14) Ballestracci, R.; Bertaut, E. F.; Pauthenet, R. *J. Phys. Chem. Solids* **1963**, *24*, 487–491.
(15) Warren, I. H.; Price, C. E. *Can. Metall. Q.* **1964**, *3*, 245–256.
(16) Sato, N.; Masuda, H.; Wakeshima, M.; Yamada, K.; Fujino, T. *J. Alloys Compd.* **1998**, *265*, 115–120.
(17) Amoretti, G.; Blaise, A.; Bogé, M.; Bonnisseau, D.; Burlet, P.; Collard, J. M.; Fournier, J. M.; Quézel, S.; Rossat-Mignod, J.; Larroque, J. *J. Magn. Magn. Mater.* **1989**, *79*, 207–224.
(18) Jin, G. B.; Raw, A. D.; Skanthakumar, S.; Haire, R. G.; Soderholm, L.; Ibers, J. A. *J. Solid State Chem.* **2010**, *183*, 547–550.
(19) Blaise, A.; Fournier, J. M.; Salmon, P.; Wojakowski, A. In *Plutonium 1975 Other Actinides, Proc. Int. Conf. 5th (1976)*; Blank, H.; Lindner, R., Eds.; North-Holland: Amsterdam, 1976; pp 635−640.
(20) Charvillat, J. P.; Wojakowski, A.; Damien, D. *Proceedings of the 2nd International Conference on Electronic Structure of the Actinides*; Ossolineum, Wroclaw, **1976**; pp 469−473
(21) Blaise, A.; Collard, J. M.; Fournier, J. M. *J. Phys., Lett.* **1984**, *45*, L-571–L-576.
(22) Wojakowski, A. *J. Less-Common Met.* **1985**, *107*, 155–158.
(23) Yoshida, Z.; Johnson, S. G.; Kimura, T.; Krsul, J. R. In *The Chemistry of the Actinide and Transactinide Elements*, 3rd ed.; Morss, L. R.; Edelstein, N. M.; Fuger, J., Eds.; Springer: Dordrecht, The Netherlands, 2006; Vol. *2*, pp 699−812.
(24) Aldred, A. T.; Dunlap, B. D.; Harvey, A. R.; Lam, D. J.; Lander, G. H.; Mueller, M. H. *Phys. Rev. B* **1974**, *9*, 3766–3779.
(25) Blaise, A.; Fournier, J. M.; Damien, D.; Wojakowski, A.; Charvillat, J. P. *J. Magn. Magn. Mater.* **1982**, *30*, 265–268.
(26) Rossat-Mignod, J.; Burlet, P.; Quezel, S.; Blaise, A.; Fournier, J. M.; Damien, D. A.; Wojakowski, A. *J. Magn. Magn. Mater.* **1982**, *30*, 122–126.
(27) Delapalme, A.; Mulak, J.; Blaise, A.; Fournier, J. M. *J. Magn. Magn. Mater.* **1982**, *30*, 117–121.
(28) Bogé, M.; Chappert, J.; Asch, L.; Kalvius, G. M.; Blaise, A.; Fournier, J. M.; Damien, D.; Wojakowski, A. *J. Magn. Magn. Mater.* **1982**, *30*, 127–134.
(29) Blaise, A.; Damien, D.; Suski, W. *Solid State Commun.* **1981**, *37*, 659–662.
(30) Thérond, P. G.; Blaise, A.; Fournier, J. M.; Chiapusio, J.; Charvillat, J. P.; Wojakowski, A. *Physica B* **1985**, *130*, 102–105.
(31) Therond, P. G.; Blaise, A.; Chiapusio, J.; Fournier, J. M.; Wojakowski, A. *J. Less-Common Met.* **1986**, *121*, 227–232.
(32) Sheft, I.; Fried, S. *J. Am. Chem. Soc.* **1952**, *75*, 1236–1237.
(33) Ionova, G. V.; Pershina, V. G.; Spitsyn, V. I. *Dokl. Akad. Nauk SSSR* **1987**, *295*, 125–126.
(34) Kaczorowski, D.; Potel, M.; Noël, H. *J. Solid State Chem.* **1994**, *112*, 228–231.
(35) Noël, H.; Zolnierek, Z.; Kaczorowski, D.; Troc, R.; Stepien-Damm, J. *J. Less-Common Met.* **1987**, *135*, 61–66.
(36) Kaczorowski, D.; Troc, R.; Noël, H. *J. Less-Common Met.* **1990**, *161*, 239–244.
(37) Gal, J.; Kroupp, M.; Hadari, Z.; Nowik, I. *Solid State Commun.* **1976**, *20*, 421–424.
(38) Gal, J.; Pinto, H.; Fredo, S.; Melamud, M.; Shaked, H.; Caciuffo, R.; Litterst, F. J.; Asch, L.; Potzel, W.; Kalvius, G. M. *J. Magn. Magn. Mater.* **1985**, *50*, L123–L127.
(39) Gal, J.; Schäfer, W.; Will, G.; Litterst, F. J.; Kalvius, G. M. *J. Less-Common Met.* **1989**, *149*, 243–247.
(40) Gal, J.; Pinto, H.; Fredo, S.; Shaked, H.; Schäfer, W.; Will, G.; Litterst, F. J.; Potzel, W.; Asch, L.; Kalvius, G. M. *Hyperfine Interact.* **1987**, *33*, 173–190.
(41) Stewart, G. R.; Kim, J. S.; Sykora, R. E.; Haire, R. G. *Physica B* **2006**, *378*−*380*, 40–43.
(42) Sarrao, J. L.; Morales, L. A.; Thompson, J. D.; Scott, B. L.; Stewart, G. R.; Wastin, F.; Rebizant, J.; Boulet, P.; Colineau, E.; Lander, G. H. *Nature (London)* **2002**, *420*, 297–299.
(43) Sakai, H.; Tateiwa, N.; Matsuda, T. D.; Sugai, T.; Yamamoto, E.; Haga, Y. *J. Phys. Soc. Jpn.* **2010**, *79*, 074721-1−5.
(44) Wells, D. M.; Jin, G. B.; Skanthakumar, S.; Haire, R. G.; Soderholm, L.; Ibers, J. A. *Inorg. Chem.* **2009**, *48*, 11513–11517.
(45) Haneveld, A. J. K.; Jellinek, F. *J. Less-Common Met.* **1969**, *18*, 123–129.

and finally air-cooled. Thin black rectangular plates of UCuOP were obtained in moderate yield, but because most of the single crystals synthesized were too small to be extracted cleanly from the product mixture, the extracted yield was less than 5 wt %. The crystals used for characterization and property measurements were manually extracted from the product mixture.

Synthesis of NpCuOP. A reaction mixture of 20.1 mg of Np (0.084 mmol), 6.7 mg of CuO (0.084 mmol), and 2.6 mg of P (0.084 mmol) was loaded into a fused-silica ampule in an Ar-filled drybox. The ampule was evacuated to $\sim 10^{-4}$ Torr and sealed. It was then placed in a computer-controlled furnace, heated to 1073 K in 24 h, kept at 1073 K for 96 h, cooled at 5 K/h to 473 K, and finally cooled at 3.67 K/h to 298 K. The resultant black powder was reloaded into a fused-silica ampule with 4 mg I_2. It was evacuated to $\sim 10^{-4}$ Torr, flame-sealed, and placed in a computer-controlled furnace where it was heated to 823 K in 8 h, kept at 823 K for 120 h, cooled at 6.42 K/h to 373 K, before finally being air cooled to room temperature. Thin black rectangular plates of NpCuOP were obtained in moderate yield, but as with UCuOP most of the crystals were very small making a clean separation from the product mixture difficult. The estimated yield of separated mass was less than 5 wt %. The crystals used in characterization were manually extracted from the product mixture.

Structure Determinations. Single-crystal X-ray diffraction data for UCuOP were collected with the use of graphite-monochromatized Mo Kα radiation (λ = 0.71073 Å) on a Bruker Smart-1000 CCD diffractometer[46] at 153 K. The crystal-to-detector distance was 5.023 cm. The data-collection strategy was determined by the program COSMO to enable collection out to $2\theta = 80°$ with high redundancy and 100% completeness.[47] The resultant strategy consisted of 0.3° scans in ω for a total of 4042 frames with 15 s/frame exposure times. The collection of the intensity data was carried out with the program SMART.[47] Cell refinement and data reduction were carried out with the use of the program SAINT,[47] and a face-indexed absorption correction along with incident beam and decay corrections were performed numerically with the use of the program SADABS.[47]

Single-crystal X-ray diffraction data for NpCuOP were collected with the use of graphite-monochromatized Mo Kα radiation (λ = 0.71073 Å) on a Bruker APEX II CCD diffractometer[46] at 100 K. The crystal-to-detector distance was 5.106 cm. The collection of the intensity data, cell refinement, and data reduction were carried out with the program APEX2.[48] A face-indexed absorption correction along with incident beam and decay corrections were performed numerically with the use of the program SADABS.[47]

The structures of both compounds were solved with the direct-methods program SHELXS and refined with the least-squares program SHELXL.[46] The program STRUCTURE TIDY[49] was then employed to standardize the atomic coordinates in each structure. Table 1 provides details of the crystal data and refinements. Further details may be found in Supporting Information.

Bond Valence Calculations. Bond valences were calculated from the standard parameters.[50]

Magnetic Susceptibility of UCuOP. DC magnetic susceptibility measurements on single crystals of UCuOP were carried out with the use of a Quantum Design MPMS5 SQUID magnetometer. The sample comprised 2.69 mg of isolated single crystals of UCuOP that were ground and loaded into a gelatin capsule. Between 3 and 300 K zero-field-cooled and field-cooled susceptibility measurements were collected with a 500 G applied field. The diamagnetic contribution of the sample holder was determined from field versus magnetization measurements to be 1×10^{-6} emu and subtracted before further analysis. The susceptibility data in the paramagnetic region were fit to the Curie−Weiss equation $\chi = C/(T - \theta_p)$, where C is the Curie constant and θ_p is the Weiss constant. The effective magnetic moment was calculated through the equation $\mu_{eff} = (7.997C)^{1/2}$ μ_B. Owing to constraints on synthesis and separation procedures, collection of NpCuOP single crystals in acceptable quantities for magnetic susceptibility measurements proved to be impossible.

Table 1. Crystal Data and Structure Refinements for UCuOP and NpCuOP[a]

	UCuOP	NpCuOP
Fw	348.54	347.51
a (Å)	3.7817(4)	3.7731(4)
c (Å)	8.225(1)	8.189(1)
V (Å^3)	117.63(2)	116.58(2)
T (K)	153(2)	100(2)
ρ_c (g cm^{-3})	9.840	9.900
μ (cm^{-1})	780.79	537.37
$R(F)^b$	0.0335	0.0199
$R_w(F^2)^c$	0.0775	0.0476

[a] For both structures $Z = 2$; space group = $P4/nmm$; λ = 0.71073 Å. [b] $R(F) = \Sigma||F_o| - |F_c||/\Sigma|F_o|$ for $F_o^2 > 2\sigma(F_o^2)$. [c] $R_w(F_o^2) = \{\Sigma[w(F_o^2 - F_c^2)^2]/\Sigma wF_o^4\}^{1/2}$ for all data. $w^{-1} = \sigma^2(F_o^2) + (q \times F_o^2)^2$ for $F_o^2 \geq 0$, where q = 0.036 for UCuOP and 0.0278 for NpCuOP; $w^{-1} = \sigma^2(F_o^2)$ for $F_o^2 < 0$.

Electrical Resistivities. The electrical resistivity and the magnetoresistivity of a single crystal of UCuOP were measured in the temperature range 0.4−300 K and in a magnetic field up to 9 T by a conventional AC four-probe technique employing a Quantum Design PPMS platform. At the lowest temperatures, the electrical current of 100 μA was used in order to avoid heating of the sample. The current was gradually increased with increasing temperature up to the value of 3 mA at room temperature.

The measured sample was a small thin platelet of the dimensions 0.5 mm × 0.11 mm × 0.01 mm. The specimen was mounted on a 0.1 mm thick sapphire plate with the use of GE/IMI 7031 varnish (Cambridge Magnetic Refrigeration). Its surface was mechanically polished using cerium oxide powder in order to remove contaminations. Subsequently, four contact pads were made by electrochemical deposition of copper from water solution of copper sulfate according to the chemical reaction: $2In + 3CuSO_4 \rightarrow 3Cu(s) + In_2(SO_4)_3$. First the specimen surface was covered by sticky tape except for the contact pads. Then, small droplets of the sulfate were placed on the exposed pads and deposition of the copper onto the sample surface was facilitated by touching these areas with indium wires. The electrical leads (30 μm thick silver wires) were attached to the so-prepared pads with silver paint.

The electrical resistivity of a single crystal of NpCuOP was measured between 2.0 and 300 K with a Quantum Design PPMS. A small rectangular plate-like crystal of NpCuOP, of dimensions 0.031 mm × 0.02 mm × 0.065 mm, was mounted along [010] with two leads in a standard linear arrangement. The leads were constructed of 15 μm diameter Cu wire, and 8 μm diameter graphite fibers that were attached with Dow 4929N silver paint. Because the minimum resistance of the sample was found to be approximately 0.16 Ω, it was assumed that the lead resistance was negligible.

Neutron Diffraction Measurements on UCuOP. Neutron diffraction experiments on UCuOP were performed on the G4.1 diffractometer installed at the Orphée reactor. The diffractometer

(46) Sheldrick, G. M. *Acta Crystallogr. Sect. A: Found. Crystallogr.* **2008**, *64*, 112–122.
(47) *Bruker, SMART Version 5.054, Data Collection and SAINT-Plus Version 6.45a Data Processing Software for the SMART System*; Bruker Analytical X-Ray Instruments, Inc.: Madison, WI, USA, 2003.
(48) *Bruker, APEX2 Version 2009.5−1 and SAINT Version 7.34a Data Collection and Processing Software*; Bruker Analytical X-Ray Instruments, Inc.: Madison, WI, USA, 2009.
(49) Gelato, L. M.; Parthé, E. *J. Appl. Crystallogr.* **1987**, *20*, 139–143.
(50) Brese, N. E.; O'Keeffe, M. *Acta Crystallogr. Sect. B: Struct. Sci.* **1991**, *47*, 192–197.

was equipped with a 800-cell multidetector system. A continuous-flow He cryostat was used. Diffraction patterns were recorded within the 2θ range of 6−86° at temperatures of 2 K, 100 K, and 228 K with neutrons of wavelength $\lambda = 2.4255$ Å. In addition, the intensities of the strongest magnetic reflections were carefully measured at several temperatures below T_N. The analysis of experimental data was made with use of the program FULLPROF. These data may be found in Supporting Information.

Theoretical Calculations. Previous theoretical methods, including the molecular field[51] and random phase Green's function[52] approximations, have been used to investigate the magnetic properties of compounds in the present tetragonal family. The application of current ab initio density functional methods using fully relativistic Dirac linear muffin-tin orbitals (LMTO) has been applied to the ferromagnetic hexagonal compound UCu_2P_2[53] and ferromagnetic $UCuP_2$,[54] but to our knowledge DFT methods have not been applied to the more complex antiferromagnetically ordered tetragonal phases. Theoretical methods similar to the ones applied here have recently been utilized in the superconducting LaFeOP system to determine band structure, Fermi surfaces, and covalency of the layered structure.[55]

Here, periodic spin-polarized band structure calculations were performed with the first principles DFT program Vienna ab initio simulation package (VASP) applying pseudopotentials with a plane-wave basis.[56−59] The exchange-correlation potential was chosen as the generalized gradient approximation (GGA) in a projector augmented wave (PAW) method.[60] Final self-consistent calculations on single unit cells also included spin orbit coupling (SOC) because the effects of such coupling can be very large for 5f orbitals and are known to shift their energies greatly. SOC was not extended to the eight unit-cell calculations owing to insufficient computing power. Automatically generated Monkhorst-Pack grids were used to carry out Brillouin-zone integrations.[61] For single unit-cell calculations $6 \times 6 \times 6$ k-point meshes were chosen for relaxations and total energy calculations; these were increased to $11 \times 11 \times 11$ k-point meshes to establish convergence, density of states (DOS), and charge distribution analysis. For the calculation of a $2a \times 2b \times 2c$ supercell of NpCuOP $4 \times 4 \times 2$ k-point meshes were chosen and increased to $6 \times 6 \times 2$ to establish convergence. Ionic relaxation convergence was established when forces on each atom relaxed below 0.02 eV/Å. With inclusion of SOC, the spin density was now coupled to the orbital angular momentum; hence, the positive (α) and negative (β) magnetization densities were coupled to the lattice vectors, and both spin (M_S) and orbital (M_L) contributions to the total magnetization (M_J) were calculated. M_L quenching was avoided by not including symmetry in all SOC calculations.[62] In order to retain the global magnetic (antiferromagnetic (AF) or ferromagnetic (F)) character of the DOS, the positive or negative density on any given atom for a given set of angular momentum numbers was summed independent of magnetization direction. The partial (pDOS) and total DOS were then found by independently summing all positive or negative density on each atom and for all atoms, respectively. The addition of the Hubbard U parameter to the current calculations could have served to shift the Fermi energies and alter the p-d-f hybridization. However, it was not included.

The electrons described as core in the PAW potentials were those composed of [Xe] $5d^{10}4f^{14}$ for U leaving 14 valence elections per atom as $5f^36s^2p^6d^17s^2$, [Xe] $5d^{10}4f^{14}$ for Np leaving 15 valence elections per atom as $5f^46s^2p^6d^17s^2$, [Ar] for Cu leaving 11 valence electrons per atom as $d^{10}s^1$, [He] for O leaving 6 electrons as $2s^2p^4$, and [Ne] for P leaving 5 electrons as $3s^2p^3$. Calculations were conducted on an 8-atom periodic crystallographic unit cell in the tetragonal space group $P4/nmm$, relaxing atomic positions within the 100 K (NpCuOP) and 153 K (UCuOP) unit cells. Owing to the unknown magnetic properties of NpCuOP, initial electronic-spin relaxations allowed for a starting moment on either one Np or one Cu to propagate throughout the unit cell. Information from these single unit-cell calculations assisted in determining the magnetic alignment in the larger supercell calculations.

The magnetic alignment of the shortest Np−Np interaction was constrained in the one unit-cell calculation by the periodic boundaries. Extension of the calculations to a $2a \times 2b \times 2c$ supercell (8 unit cells, 64 atoms, 592 electrons) removed the ferromagnetic constraint on the closest Np atoms. The difference in energy between magnetic states was small and convergence was reached very slowly. The previously described method of magnetic moment propagation[63] proved to be problematic. Thus, additional model ferromagnetic and antiferromagnetic alignments were initialized. Four models were constructed wherein the Np layers were ferromagnetic but were stacked in different configurations: AFI (+ − + −), AFII (+ − − +), AFIII (+ + − −), and ferromagnetic F (+ + + +). Examples of antiferromagnetic ordering within the An layers have not been demonstrated for this series of compounds, but for completeness model AFIV was initialized with the first and second closest Np−Np interactions having opposite spins.

Oxidation states were investigated through the use of electron density surfaces determined by volume integration with the use of both "Wigner Seitz radii" R_{ws} and Bader's topological atom method.[64,65] Rather than dividing space into hard spheres (R_{ws}), the approach of Bader is to divide space into atomic regions determined by zero-flux charge-density surfaces.[64] The accuracy of the charge distribution was established by increasing the size of the fast-Fourier-transform mesh until the difference in Bader charge on an atom between any two calculations was less than 0.003 electrons. Using these two methods, we define the oxidation state as the difference between the number of valence electrons contained within a volume and the number assigned to the neutral atom. The values of R_{ws} were initially set to the standard crystal radii[66] of the atom and manipulated to maximize the percentage of the unit cell volume contained by the spheres. The final radii used were UCuOP: 1.5 Å for U, 1.1 Å for Cu, 1.5 Å for O, and 1.8 Å for P; NpCuOP: 1.31 Å for Np, 1.25 Å for Cu, 1.5 Å for O, and 1.9 Å for P. In addition to oxidation state analysis, R_{WS} integrations were utilized within VASP for the separation of charge for pDOS and local magnetic moment determinations.

Results

Experimental Structure. The low-temperature (153 K) structure of UCuOP determined here differs very little

(51) Przystawa, J.; Suski, W. *Phys. Status Solidi A* **1967**, *20*, 451–459.
(52) Przystawa, J. *Phys. Status Solidi A* **1967**, *24*, 313–322.
(53) Antonov, V. N.; Harmon, B. N.; Yaresko, A. N.; Perlov, A. Y. *Phys. Rev. B* **1999**, *59*, 14571–14582.
(54) Horpynyuk, O.; Nemoshkalenko, V. V.; Antonov, V. N.; Harmon, B. N.; Yaresko, A., N. *Low Temp. Phys.* **2002**, *28*, 533–538.
(55) Lebègue, S. *Phys. Rev. B* **2007**, *75*, 035110/1–035110/5.
(56) Kresse, G.; Hafner, J. *Phys. Rev. B* **1993**, *47*, 558–561.
(57) Kresse, G.; Hafner, J. *Phys. Rev. B* **1994**, *49*, 14251–14271.
(58) Kresse, G.; Furthmüller, J. *Comput. Mater. Sci.* **1996**, *6*, 15–50.
(59) Kresse, G.; Furthmüller, J. *Phys. Rev. B* **1996**, *54*, 11169–11186.
(60) Kresse, G.; Joubert, D. *Phys. Rev. B* **1999**, *59*, 1758–1775.
(61) Monkhorst, H. J.; Pack, J. D. *Phys. Rev. B* **1976**, *13*, 5188–5192.
(62) Fazekas, P. *Series in Modern Condensed Matter Physics: Lecture Notes on Electron Correlation and Magnetism*; World Scientific Publishing Co. Pte. Ltd.: River Edge, NJ, 1999; Vol. *5*.
(63) Yao, J.; Wells, D. M.; Chan, G. H.; Zeng, H.-Y.; Ellis, D. E.; Van Duyne, R. P.; Ibers, J. A. *Inorg. Chem.* **2008**, *47*, 6873–6879.
(64) Henkelman, G.; Arnaldsson, A.; Jónsson, H. *Comput. Mater. Sci.* **2006**, *36*, 354–360.
(65) Sanville, E.; Kenny, S. D.; Smith, R.; Henkelman, G. *J. Comput. Chem.* **2007**, *28*, 899–908.
(66) Shannon, R. D. *Acta Crystallogr. Sect. A: Cryst. Phys. Diffr. Theor. Gen. Crystallogr.* **1976**, *32*, 751–767.

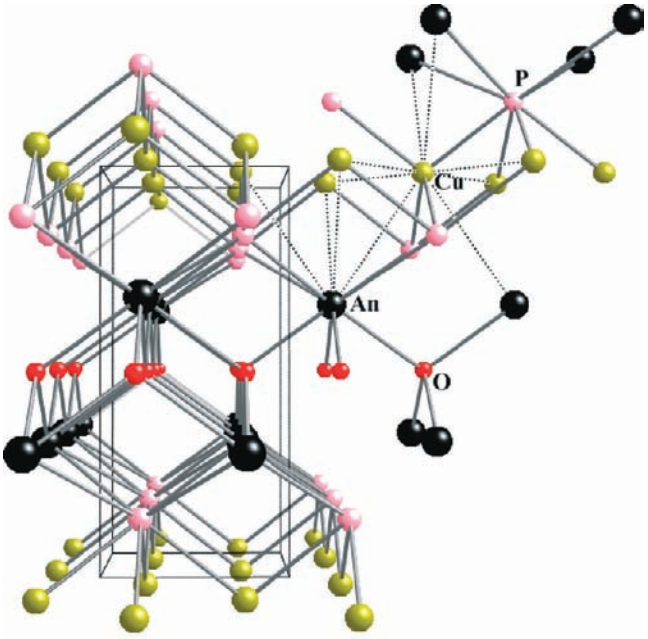

Figure 1. The structure of AnCuOP compounds viewed down [010].

from those previously determined at room temperature.[3,43] NpCuOP at 100 K is isostructural with the U compound; the change in *z*-coordinates of the An and P atoms sitting on the 2*c* Wyckoff positions is less than 0.002 Å. Crystallographic and refinement information can be found in Table 1. As in the previously determined structures,[3,43] the An atoms are coordinated to four O and four P atoms forming a distorted square antiprism. The antiprisms face share in the *ab*-plane and edge share through O atoms in the *c*-direction (Figure 1). The face- and edge-sharing interactions generate two relatively short An−An interactions of 3.7817(4) and 3.8129(9) Å.

Because the bonding in UCuOP was described previously,[3] comparisons of metrical data (Table 2) to those in other compounds are made only for NpCuOP. The Np−O interatomic distance at 2.3139(3) Å is comparable to those found in NpO_2 (2.3539(3) Å)[67] and NpOS (2.3249(2) Å).[18] The Np−P interatomic distance at 2.965(1) Å is longer than that in NpPS (2.777 Å)[20] or NpP (2.8073(1) Å).[68] The face-sharing interaction in the *ab*-plane generates four short intralayer An−An interactions, J_1, at 3.7731(4) Å. As with the cation−anion interactions, this Np−Np interaction is shorter but comparable to those of NpOS (3.8088(3) Å)[18] and NpPS (3.807 Å).[68] It is much shorter than that of NpP (3.970 Å)[68] or $NpAs_2$ (3.930 Å).[69] In the edge-sharing *c*-direction the interlayer Np−Np distance, J_2, is only slightly longer than the intralayer distance at 3.7813(6) Å. As NpOS crystallizes in the related PbFCl structure-type, this same edge-sharing interaction is present at 3.7902(4) Å.[18] The Cu−Cu distance is 2.6680(3) Å and the Np−Cu distance is 3.3387(4) Å. The Np−Cu distance is longer than that in the intermetallic compound $NpCu_2Ge_2$ (3.2666(7) Å)[39] but shorter than that in $NpCu_4Al_8$ (3.359(1) Å).[38]

(67) Zachariasen, W. H. *Acta Crystallogr.* **1949**, *2*, 388–390.
(68) Mueller, M. H.; Lander, G. H.; Knott, H. W.; Reddy, J. F. *Phys. Lett. A* **1973**, *44*, 249–250.
(69) Wojakowski, A.; Damien, D. *J. Less-Common Met.* **1982**, *83*, 263–267.

Table 2. Selected Interatomic Distances (Å) and Angles (deg) for UCuOP and NpCuOP[a]

	UCuOP	NpCuOP
An−O × 4	2.3286(4)	2.3139(3)
An−P × 4	2.968(2)	2.965(1)
An−Cu × 4	3.3403(6)	3.3387(4)
An−An × 4	3.7817(4)	3.7731(4)
An−An × 4	3.8129(9)	3.7814(6)
Cu−P × 4	2.392(3)	2.386(2)
Cu−Cu × 4	2.6741(3)	2.6680(3)
O−An−O	70.09(1)	70.411(9)
O−An−O	108.59(2)	109.24(2)
O−An−P	74.69(6)	74.57(4)
O−An−P	140.40(3)	140.48(2)
P−An−P	79.15(6)	79.02(4)
P−An−P	128.6(2)	128.25(9)
P−Cu−P	104.4(2)	104.5(1)
P−Cu−P	112.05(8)	112.01(5)

[a] Some comparative interatomic distances in ThCuOP[43] are Th−O = 2.3892(5), Th−P = 3.060(2), Cu−P = 2.424(3) Å.

In UCuOP the unit-cell volume decreases from 118.4 $Å^3$ at room temperature[3] to 117.63(2) $Å^3$ at 153 K (Table 1). This volume decrease shortens the closest U−U interactions from 3.793(1) at 298 K to 3.7817(4) Å at 153 K. The second closest U−U interaction is also reduced from 3.825(1) to 3.8129(8) Å. The standard crystal radius[66] for eight-coordinate U^{4+} is 0.02 Å longer than that for eight-coordinate Np^{4+}. No differences this large are seen in Table 2; any differences there would actually have been smaller had the two structures been determined at the same low temperature.

Bond Valences. The calculated bond valencies for UCuOP are 3.9, 1.3, −2.2, and −2.9 for U, Cu, O, and P, respectively. Such empirical bond-order sums depend solely on available bond lengths. In the present instance, because U +4 is found more often than U +3 in such solid-state compounds the results will probably be biased in favor of U 4+. With that caveat, the results support the formulation of UCuOP as $U^{4+}Cu^{1+}O^{2-}P^{3-}$. Note that bond valence sums are most closely related to "valency", that is, to the number of bonds formed, and not to "charge". Charge distributions are discussed below.

Magnetic Susceptibility of UCuOP. The temperature-dependent magnetic susceptibility (χ) of UCuOP, as determined from ground single crystals, is displayed in Figure 2. In agreement with the previous study on polycrystals,[3] the compound displays antiferromagnetic ordering at 224(2) K, but it is clear that the low temperature (80 K) anomaly reported earlier[3] is neither present in the current sample nor in that measured by Sakai et al.[43] The original analysis of the magnetism of UCuOP discussed three possible origins for the low-temperature upturn and inflection: $UCuP_2$ impurities, $UCuP_2$ and UCuOP crystal intergrowth, or spin canting intrinsic to UCuOP. Even though small changes in synthesis of the current sample could lead to different types of crystals and a lack of $UCuP_2$ and UCuOP intergrowth, it seems more likely that the original sample contained trace quantities of $UCuP_2$ that were undetectable by powder X-ray diffraction methods.

Application of the Curie−Weiss law to the paramagnetic region between 244 and 300 K yields an estimation of the effective moment $\mu_{eff} = 2.82(2)\,\mu_B$. This moment is smaller than μ_{eff} calculated from free-ion moments for

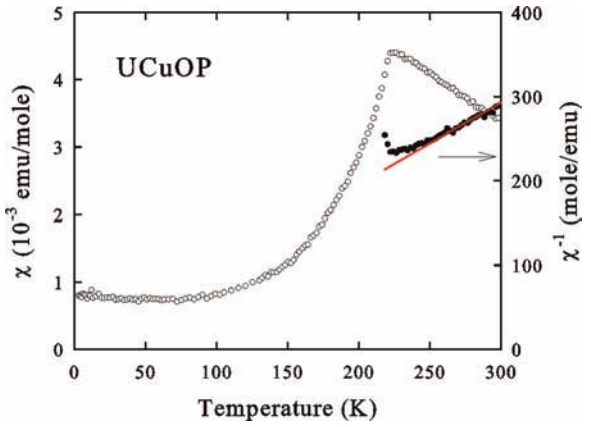

Figure 2. Magnetic susceptibility (χ) vs temperature of UCuOP measured on powdered single crystals in a field of 0.5 T. The right axis refers to the inverse susceptibility. The line is the Curie−Weiss fit.

U^{4+} (3.58 μ_B) and U^{3+} (3.62 μ_B) models,[70] but is reasonable considering the previously reported value of 2.68 μ_B[3] and those of the related compounds UP_2 (2.30 μ_B),[6,7] $UCuP_2$ (2.53 μ_B),[11] and $U_2Cu_2OP_3$ (2.66 μ_B).[36] The use of free-ion moments to calculate μ_{eff} and assist in assigning oxidation states is problematic in solid-state actinide compounds where the effects of crystal-field splitting can be very pronounced.

On the other hand, from measurements on a single crystal, Sakai et al.[43] found T_N = 220 K with values of μ_{eff} = 3.6 μ_B for the field along the *a* and *c* axes. The corresponding Weiss temperatures are −1000 and −60 K, respectively. The magnitude of χ in the paramagnetic region above T_η is about twice that measured along the *c* axis in the present study although at 4.2 K there is little difference. This may reflect differences in the two samples.

Electrical Resistivities. The temperature-dependent electrical resistivities in the basal plane ($i \perp c$) of UCuOP and NpCuOP single crystals are displayed in Figures 3 and 4, respectively. Both display resistive anomalies in the low-temperature regions that are similar to those seen in UP_2 and $U_2Cu_2OP_3$.[9,36,71]

The basal plane resistivity ($\rho_\perp$) of UCuOP displayed in Figure 3 is very similar to that of UP_2[9] and $UCuP_2$[10] measured for the same configuration of the electrical current with respect to the crystallographic axes. At 299 K, the resistivity is 745 $\mu\Omega$ cm. In the paramagnetic region, between 205 and 300 K, the resistivity can be fit to the equation $\rho_\perp = A + c_{ph}T$, where A = 668.6(3) $\mu\Omega$ cm and c_{ph} = 0.253(2) $\mu\Omega$ cm/K. If we assume that the Matthiesen rule applies, then A is the sum of the residual resistivity from defects and the spin-disorder resistivity.[9] The parameter c_{ph} describes the resistance from electron−phonon drag; its value is an order of magnitude higher than that of UP_2 (0.073 $\mu\Omega$ cm/K).[9] Below 80 K, the resistivity can be fit to the formula $\rho_\perp = \rho_0 + c_m T^2 \exp(-\Delta/T)$, appropriate for the antiferromagnetically ordered region probed by the electric current flowing perpendicular to the magnetic moments. Here ρ_0 stands for the residual resistivity and Δ represents a gap in the spin-wave spectrum. The least-squares fitting yielded the

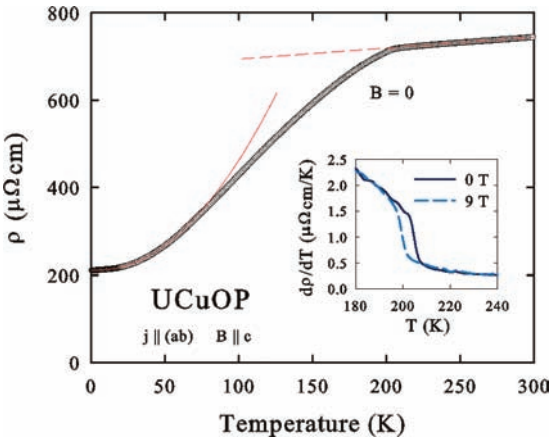

Figure 3. Electrical resistivity vs temperature of UCuOP measured with the current perpendicular to the *c*-axis. The solid and dashed curves are the fits discussed in the text. Inset: derivative of the resistivity with respect to temperature in the vicinity of the transition taken in zero field and in a field of 9 T applied along the *c*-axis.

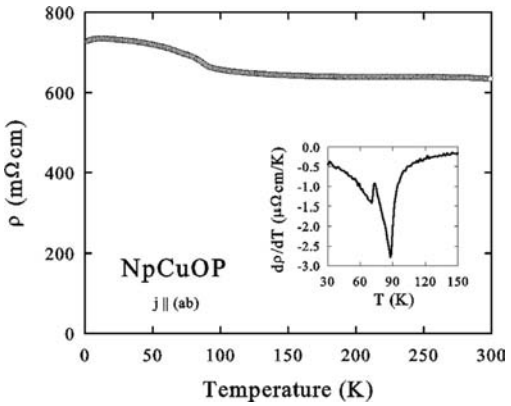

Figure 4. Electrical resistivity vs temperature of NpCuOP measured along the *b* axis. Inset: derivative of the resistivity with respect to temperature in the vicinity of the transition.

parameters ρ_0 = 211.7(2) $\mu\Omega$ cm, c_m = 0.028(1) $\mu\Omega$ cm/K^2, and Δ = 10.5(3) K. Subtracting ρ_0 from A gives an estimate of the spin-disorder resistivity at high temperatures to be about 457 $\mu\Omega$ cm.

A plot of the derivative of resistivity with respect to temperature (inset Figure 3) exaggerates the effect of magnetic ordering on the resistivity and allows for the determination of T_N. The resultant value of T_N is approximately 10 K below the value of 224 K determined from the magnetic data. The difference between these two temperatures can be attributed to the somewhat different sensitivities of the two properties to short-range magnetic order.[36] At a magnetic field of 9 T, the value of T_N is reduced to 204 K. Reduction of the critical temperature with the application of magnetic field is a characteristic feature of antiferromagnets.

The transverse magnetoresistance (MR) of UCuOP displayed in Figure 5, defined as MR = $[\rho(B) - \rho(B = 0)]/\rho(B = 0)] \times 100\%$, measured with the electric current flowing in the basal tetragonal plane and the magnetic field applied along the *c*-axis. The MR response is very small; its absolute value does not exceed 1% in 9 T for any temperature. In the paramagnetic state, MR is negative and varies approximately as B^2. In the ordered region,

(70) Kittel, C. *Introduction to Solid State Physics*, 7th ed.; Wiley: New York, 1996.
(71) Schoenes, J.; Kaczorowski, D.; Beeli, C. *Z. Phys.* **1992**, *B88*, 135–140.

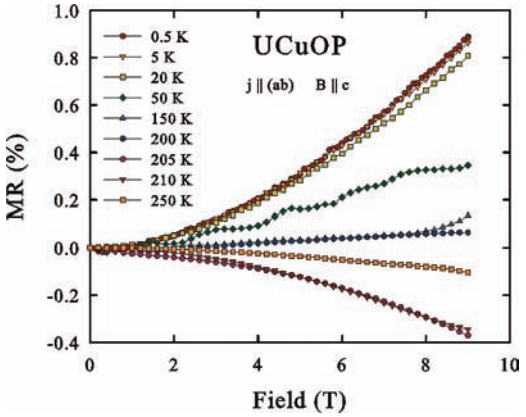

Figure 5. Transverse magnetoresistance isotherms of UCuOP with the current flowing in the basal plane.

one observes a change in the sign of MR from positive at low temperatures to negative close to T_N, and the MR isotherms also have a B^2-like shape. Such a behavior is characteristic of antiferromagnetic systems.[72]

Sakai et al.[43] have also measured the electrical resistivity of a single crystal of UCuOP. Their results exhibit an order of magnitude higher resistivity than the present study and an abrupt increase just below T_N which is not present in our results. These differences once again may reflect differences in the two samples or be a manifestation of the experimental procedures. Surface oxidation, which would lead to higher resistance, was scrupulously avoided in our study; sample preparation was not discussed by Sakai et al.

The measured basal-plane resistivity of NpCuOP is nearly 640 mΩ cm at 298 K. This value can be compared to the resistivity of single-crystalline $NpAs_2$ of only 95 μΩ cm at 298 K.[30] Even though the resistance of the leads in this two-probe measurement does contribute to the overall resistivity, it should be low compared to the large resistivity determined here. Down to about 90 K, $\rho_\perp$ hardly changes with temperature. Below this temperature the $\rho_\perp(T)$ curve forms a broad hump, reminiscent of the behavior of antiferromagnets possessing magnetic unit cells larger than their crystallographic unit cells. This characteristic anomaly in the electrical conduction arises from excess conduction electron scattering on the "magnetic Brillouin zone" boundaries. As shown in the inset to Figure 4, the derivative of the resistivity of NpCuOP with respect to temperature exhibits a sharp minimum at 90 K. The shape of this feature supports the hypothesis that the compound undergoes a transition into an antiferromagnetically ordered state. Similar behavior has been reported, for example, for antiferromagnetic $U_2Cu_2OP_3$,[71] yet in the latter compound it occurs for the resistivity measured along the tetragonal *c*-axis, whereas for NpCuOP it is observed for the basal plane. It is unfortunate that the limited availability of NpCuOP prevents further experimental studies; any quantitative analysis of its interesting electronic and magnetic properties is not possible at this time.

Neutron Diffraction Measurements on UCuOP. Neutron diffraction powder data led to a crystal structure for UCuOP that is in good agreement with those determined by X-ray diffraction single-crystal methods here and previously.[3] The magnetic diffraction patterns taken at 2 and 100 K were fully indexable on the basis of the chemical unit cell. The observed additional (10*l*) magnetic reflections are characteristic of collinear antiferromagnetic ordering of the AFI type. Thus, the magnetic structure of UCuOP consists of ferromagnetic (001) layers of U atoms stacked along [001] in the sequence + − + −. The magnetic moments are also aligned along [001]. At 2 K the uranium magnetic moment is 2.42(6) μ_B. The temperature dependence of the (100) magnetic peak intensity is shown in Figure 6. It yields a value of T_N of about 220 K, in agreement with the results from magnetic susceptibility measurements

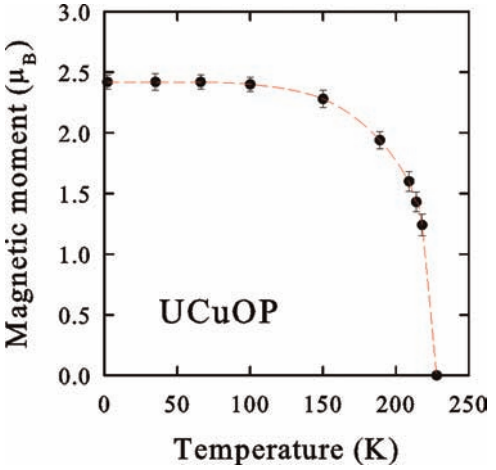

Figure 6. Temperature variation of the ordered magnetic moment in UCuOP.

Theoretical Relaxed Ionic and Magnetic Structures. During relaxation of the atoms within the 153 K crystallographic unit cell of UCuOP, the U atoms moved less than 0.02 Å toward the O layer and the P atoms moved less than 0.004 Å toward the Cu layer. The Cu and O layers remained stationary owing to symmetry constraints. After the relaxed positions in the LSDA + GGA method were determined, SOC was implemented. Taking the crystallographic [001] as the axis of magnetization, antiferromagnetic total magnetic moments of 1.40 μ_B and $M_L = 2.03\ \mu_B$, both aligned along [001], were found for the two U atoms. The electronic configuration of U using R_{WS} values was $6d^{0.8}5f^{2.6}$, whereas for Cu it was $3d^{8.9}$. These values clearly approach $5f^3$ for U^{3+} and $3d^9$ for Cu^{2+}. For Cu^{2+} a magnetic moment is expected, but the calculated magnetic moment here was only 0.004 μ_B. At 1.40 μ_B, the total U magnetic moments were nearly half the experimental value of 2.42(6) μ_B by neutron diffraction measurements. However, the calculated U moment is considerably less than the free ion moments of 3.58 μ_B for U^{3+} and 3.62 μ_B for U^{4+}, in agreement with the experiments. The reason for the underestimated total moment may well lie in errors in the calculated coupling between orbital (L) and spin (S) moments, which in the present scheme is done perturbatively. The fact that the Cu d-electron count is less than 10 e^- is not necessarily an indicator of localized magnetization; in fact, the partial density of states and charge maps show strong Cu−P covalency (see below). In this case the local exchange interaction, which would favor a Cu moment, is overwhelmed by

(72) Yamada, H.; Takada, S. *J. Phys. Soc. Jpn.* **1973**, *34*, 51–57.

the stronger ligand field. Incorporation of the Hubbard U term for electron−electron coupling could increase the magnetic moments, but to do this is beyond the scope of the present work. In addition, the magnetic moments and f-electron counts are dependent on the selected R_{WS} values. Increasing R_{WS} could increase the per-U magnetic moments but would also increase overlap with O and P and cause double counting of electrons.

Single Unit Cell of NpCuOP. When a moment on one Np or Cu atom was allowed to propagate throughout one crystallographic unit cell, then only the Np atoms possessed significant magnetization greater than 0.1 μ_B. The crystallographic unit cell contains two An positions so two magnetic configurations are possible, ferromagnetic and antiferromagnetic. During relaxation of the atoms within the 100 K crystallographic unit cell of NpCuOP, the Np atoms moved toward the central O layer by 0.01 Å for the antiferromagnetically (AF) aligned and 0.03 Å for the ferromagnetically (F) aligned configuration. The P atoms moved toward the Cu layer and away from the Np atoms by 0.02 Å for the AF calculation and 0.01 Å for the F calculation. Cu and O atoms were again stationary owing to symmetry constraints.

Taking the [001] crystallographic axis as the axis of magnetization for both AF and F cases, we found the F model to be lower in energy by 35 meV. Before the inclusion of SOC, the energy difference between the magnetic structures was more than 10 times larger at 380 meV. In the F structure, the calculated total magnetic moments (M_J) on each Np center are 2.87 μ_B. The electronic configuration of Np with the use of R_{WS} is $6d^{0.6}5f^{3.7}$, whereas Cu is $3d^{8.6}$. As in UCuOP, these values clearly approach $5f^4$ for Np^{3+} and $3d^9$ for Cu^{2+}. Even though the calculated Cu magnetic moment here is only 0.06 μ_B, this is more than 10 times larger than that calculated for Cu in UCuOP. Our interpretation is that the small Cu moments are the result of polarization by the An local moments, the larger Np moment driving a correspondingly larger Cu polarization. As mentioned above, the strong Cu-P covalency suppresses the formation of local Cu moments by the intraatomic exchange. The other atoms of the structure were determined to have magnetic moments only along the [001] axis of less than 0.1 μ_B and are listed in Table 3. Even though small, the moment on the O atom is coupled parallel to the Np layers, whereas that of Cu and P have opposite magnetizations.

Supercell Calculations on NpCuOP. In order to remove the ferromagnetic constraint on the nearest Np−Np interaction, J_1, the calculations were extended to a $2a \times 2b \times 2c$ supercell. The relative energies of each magnetic model for the supercell calculations may be found in Table 4. In these five models for NpCuOP in a $2a \times 2b \times 2c$ supercell, the ferromagnetic alignment (F) of Np moments was also the lowest in energy by more than 0.79 eV (Table 4). As occurred in the single-cell calculations, incorporation of SOC could, of course, reduce the magnitude of this energy difference between the models. Compared to the diffraction results, the Np atom moved on average 0.05 Å toward the nearest O layer and the P atom moved 0.01 Å toward the nearest Cu layer. The Cu and O atoms remained stationary owing to symmetry constraints. The Np movement was slightly larger than in the single unit-cell case, but we consider such movement to have little effect on the final results.

Table 3. The Calculated Spin (M_S), Orbital (M_L), and Total Magnetic Moments M_J (μ_B) of NpCuOP

	M_S	M_L	M_J
Np[a]	5.58	−2.71	2.87
Cu	−0.07	0.01	−0.06
P	−0.01	−0.09	−0.1
O	0.00	0.01	0.01

[a] Magnetization direction taken as [001].

Table 4. Calculated Total Energies (E_v) Relative to the Lowest Energy Structure and the Average Magnitude of the Magnetic Moments (M) for Each Magnetic Arrangement for NpCuOP

NpCuOP	AFI	AFII	AFIII	AFIV	F
ΔE	2.92	2.26	0.79	2.87	0.00
M	3.0(1)[a]	3.0(4)	3.15(6)	3.03(10)	3.10(6)

[a] Standard deviations are large owing to differences in neighboring layers of Np atoms.

Table 5. Calculated Average Magnitude of Np Magnetic Moments (M_j) for Layers of Np Atoms at z = 1/6, 1/3, 2/3, and 5/6 of the $2a \times 2b \times 2c$ Supercell of NpCuOP

z	AFI	AFII	AFIII	AFIV[a]	F
1/6	3.16(1)	3.12(1)	3.22(5)	3.10(8)	3.16(1)
1/3	3.1(1)	3.3(6)	3.18(5)	3.14(6)	3.14(7)
2/3	2.94(1)	2.62(1)	3.09(1)	2.95(1)	3.05(1)
5/6	2.93(2)	2.9(2)	3.10(1)	2.94(2)	3.04(1)

[a] For AFIV averages are of positive spins in the first four unit cells (z = 1/6 and 1/3) then the second four unit cells (z = 2/3 and 5/6).

Interestingly, in all supercell calculations the Np magnetic moments decrease between neighboring Np layers (Table 5). In the ferromagnetic supercell calculation the first two layers in the c-direction average to 3.15(5) μ_B, whereas the second two average to 3.04(1) μ_B, moving away from the origin. The decrease in Np moment could be indicative of modulated antiferromagnetic ordering such as found experimentally in $NpAs_2$.[26] Further attempts to tease out this type of interaction through calculations of ferromagnetic alignment in supercells of $a \times b \times 2c$ and $a \times b \times 4c$ did not produce the same arrangements, suggesting the importance of the intralayer J_1 interactions. Even though the resistivity trend determined here suggests some type of AF ordering in NpCuOP, the actual configuration of the magnetic moments could not be determined. The "hump" in the basal-plane resistivity conflicts with that determined for the U members of the family, and therefore the following analyses of the DOS and charge distribution for NpCuOP will use the lowest-energy ferromagnetic alignment of Np ions.

Density of States of UCuOP. A plot of the total DOS and partial DOS (pDOS) including spin−orbit coupling for each atom type in UCuOP is found in Figure 7. The states surrounding the Fermi energy, E_F, (set to 0 eV) from approximately −2.5 to 2 eV are dominated by U states with small contributions from all other species. The contribution from the U-6d orbitals in this region is small suggesting minimal hybridization with the U-5f orbitals. The states above −0.5 eV are almost exclusively those from 5f-states where there are five regions of band overlap (peaks), one below and four above E_F. The increased

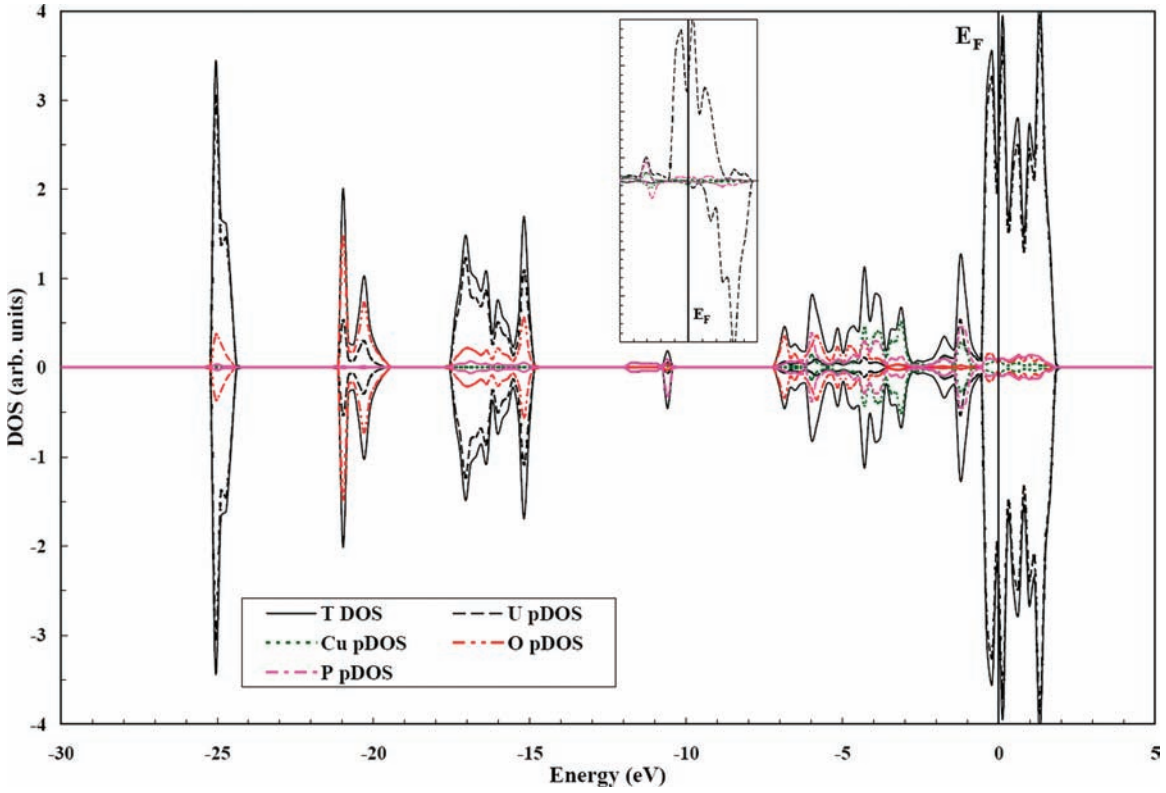

Figure 7. Total DOS and pDOS for UCuOP. The Fermi level is at 0 eV. Inset displays pDOS for magnetically coupled U1, P1, and Cu1 atoms surrounding the Fermi energy.

width of the peak below E_F is due to partial overlap of filled bands of f_{xz^2} and f_{yz^2} character. Above E_F the majority component of the four peaks is from empty $f_{x(x^2-3y^2)}$ and f_{zxy} states and antibonding f_{xz^2} and f_{yz^2} states. The $f_{y(3x^2-y^2)}$, f_{z^3}, and $f_{z(x^2-y^2)}$ states are partially filled forming wide bands ranging from approximately −0.5 to 0.8 eV. Their antibonding states overlap with those of f_{xz^2} to form the highest plotted bands at 1.3 eV.

The symmetric nature of total DOS results from the summed contributions from both α- and β-magnetizations. For atom U1 (3/4, 3/4, 0.34) the majority bands at E_F are α-states, but the unoccupied antibonding states above E_F have β-magnetization, inset to Figure 7. E_F crosses the bands at a region of high α-magnetization density suggesting UCuOP is actually semimetallic within the U layers. The small β-density at approximately 0.12 eV suggests a complex interaction between α- and β-states and consequently the AF aligned U-layers. Incorporation of an onsite Coulomb correction term would likely split these f-bands, but as the resistivity displays complex metallic-like character it is possible the overlap would be retained. Shifting of sub-bands around E_F would occur, with changes in the absolute value of the DOS at E_F. However, it is doubtful that a simple counting of states is adequate to describe any transport property of such a heavy fermion system. It must be kept in mind that the Hubbard U parameter must presently be considered as empirical and adjusted to fit some physical property.

Between −2.5 and −0.5 eV is a region of enhanced interaction between U, P, and Cu. The contribution from P has both p- and d-character that is significantly coupled to the U density. This can be seen in the inset to Figure 7 where along with the pDOS of U1, those of P1 (1/4, 1/4, 0.18) and Cu1 (3/4, 1/4, 0) are plotted. The P 3p majority states are stabilized and shifted to lower energy by overlapping with the U 5f-states, whereas the P 3p minority states are shifted to higher energy mirroring the U 5f (above E_F). There are contributions from several f-orbitals at this energy, but the major contribution is fittingly from f_{zxy} as the lobes of the axially quantized representation for this orbital point toward the corners of a cube. It should interact with the P electrons in an σ-bonding fashion. The P density at this energy is also coupled to the Cu layer where the pDOS of Cu1 displays a similar shifting of the majority α-states to lower binding energy whereas the minority β are shifted slightly higher. Figure 8 is a three-dimensional representation of the magnetization density; the coupling between U and P can clearly be seen in the small lobe (blue) above P1 and toward the itinerate U-f density around U1 (red). A similar amount of magnetization is located around the O atoms, but they are coupled to both α- and β-magnetization f-density. The coupling between U1 and Cu1 is likely the result of super exchange through P.

The majority of the Cu-3d states are located between −4.5 and −2.5 eV and overlap with the P-3p states that extend down to −7 eV. The region from approximately −7 to −4.5 eV contains contributions from all species, but the major contribution is from the O and P anions. The four regions of overlap at higher binding energies are mainly from U-anion overlap. The peak and shoulder at approximately −11 eV are from P-3s density with small contributions from both Cu and U. The three regions between −25 and −14.5 eV are predominately from overlap of U-6p, O-2s, and O-2p-states. As with the U−P overlap near E_F, the density at these higher binding energies is also asymmetric within a ferromagnetically aligned

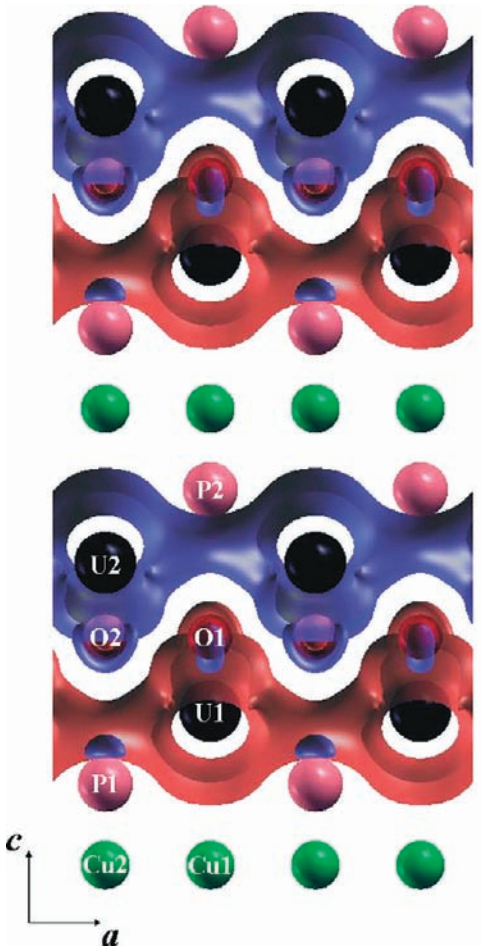

Figure 8. Isosurface plot of the magnetization distribution in UCuOP with an isovalue of 0.01. An eight unit cells supercell ($2a \times 2b \times 2c$) is shown. The view is down [010]. In the figure, α-magnetization density (red) and β-magnetization density (blue) are plotted along with U (black), Cu (green), O (red), and P (pink).

U layer (not shown). The region from approximately −17.5 to 14.5 eV is from U-6p overlap with both O-2s (−16 to −14.5 eV) and O-2p (−17.5 to −16 eV). There is also a small contribution from the P-3s and P-3p in this region. The two regions at approximately −20 and −25 eV are again from U-6p and O-2s, but there are no contributions from the O-2p state.

Density of States of NpCuOP. A plot of the DOS and pDOS including spin−orbit coupling for an F single unit cell of NpCuOP can be found in Figure 9. As in UCuOP, the states surrounding the Fermi level from approximately −0.5 to 3 eV are predominately 5f states, but the contributions from the other species are much more significant. The significant Np 6d contributions in this region mirror the shape of the 5f-states and suggest some degree of 5f-6d hybridization. In the U compound, the 5f-orbitals were further split allowing differentiation of the orbitals into filled, partially filled, and empty states, but in the Np analogue the 5f states form almost completely degenerate wide bands with contributions from all the orbitals in each DOS peak near E_F. The partially filled Np-5f bands at E_F and the shifting of the minority (β) magnetization states to above E_F suggest that NpCuOP is also semimetallic. Even though there is extensive evidence of hybridization of the orbitals at E_F, the higher binding energy overlap regions are similar to those found in UCuOP. The features between −0.5 and −2 eV are from overlap of Np, Cu, and P bands where the majority α-states are stabilized in energy, whereas the β-states are shifted to higher energy. Even though the contribution from all Np f-orbitals at this energy is much more evenly divided than are the f-orbitals of U, the f_{zxy} orbital again has the largest contribution. The enhanced asymmetry in the P-pDOS between −12 and −10 eV emphasizes the AF coupling of these p-states with Np as the β-states are stabilized to lower energy whereas the α-states are shifted to higher binding energies. The AF coupling of the magnetization density is also evident in the three-dimensional representation of the magnetization density, Figure 10, where the itinerant Np magnetization density forms layers in the (001) plane (red), and the other atoms are surrounded by density of magnetization opposite that of the Np ions (blue).

Comparison of DOS between 4f and 5f Compounds. The electronic states surrounding the Fermi level in these actinide compounds are very different from those calculated for the isostructural rare-earth oxypnictide compounds. Calculations on LaFeOP,[55] LaFeOAs,[73,74] and LnFeOAs (Ln = La, Ce, Pr, Nd, Sm, and Y)[75] show the Fermi energy to be dominated by Fe-3d states, whereas the Ln-4f states are much higher in binding energy. An extensive ab initio study found that rare-earth substitution should have very little effect on the electronic structure, and suggested that any magnetic interactions between Ln and FeAs layers would be weak.[75] The limited involvement of the rare-earth in the properties of these compounds is also emphasized by the observation of superconductivity not only in the LnFeOAs compounds but also in the related AFe_2As_2 (A = K, Cs, K/Sr, Cs/Sr, Ba, and Sr) compounds.[75−77] The electronic properties of the actinide compounds investigated here are dominated by the 5f states at the Fermi energy and by the magnetic ordering of the 5f-electrons. The Cu-3d states in these compounds are pushed down below the Fermi level where they overlap with O-2p and P-3p states. The more diffuse 5f-orbitals also show enhanced overlap with both O and P states at the Fermi energy and at higher binding energies when compared to Ln-O or Ln-P overlap.[73] As such, none of these rare-earth or actinide structures should be viewed as containing isolated LnO or AnO and MT layers.

Theoretical Charge Distribution. Assignment of formal oxidation states in actinide compounds is complicated by delocalization of 5f-electrons and covalent bonding. The calculated average charge on each atom from both R_{WS} integration and the Bader topological method may be found in Table 6. The charges determined from R_{WS} are over one electron short of the total for both compounds; this suggests considerable delocalization into the interstitial region. Therefore, Bader charges are now discussed.

(73) Singh, D. J.; Du, M.-H. *Phys. Rev. Lett.* **2008**, *100*, 237003/1–237003/4.
(74) Wojdel, J. C.; Moreira, I.; de, P. R.; Illas, F. *J. Am. Chem. Soc.* **2009**, *131*, 906–907.
(75) Nekrasov, I. A.; Pchelkina, Z. V.; Sadovskii, M. V. *JETP Lett.* **2008**, *87*, 560–564.
(76) Chen, G. F.; Li, Z.; Wu, D.; Li, G.; Hu, W. Z.; Dong, J.; Zheng., P.; Luo, J. L.; Wang, N. L. *Phys. Rev. Lett.* **2008**, *100*, 247002−1-4.
(77) Sasmal, K.; Lv, B.; Lorenz, B.; Guloy, A. M.; Chen, F.; Xue, Y.-Y.; Chu, C.-W. *Phys. Rev. Lett.* **2008**, *101*, 107007−1-4.

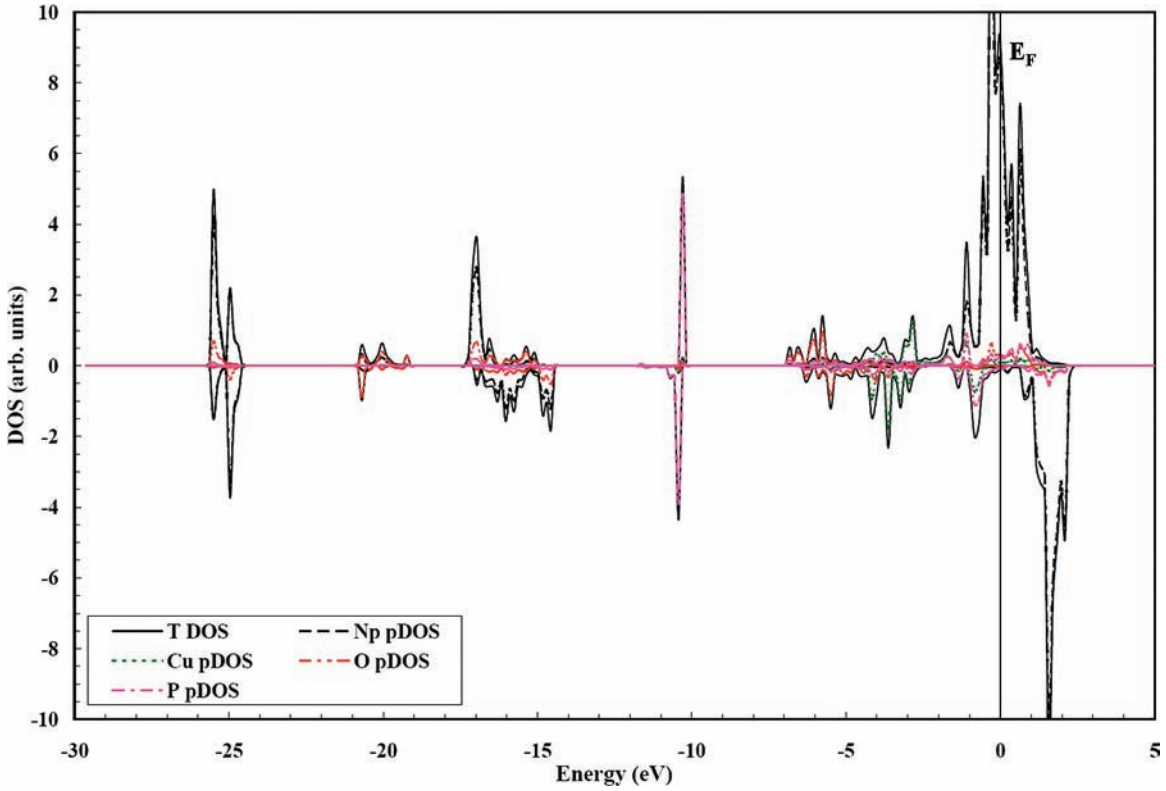

Figure 9. Total DOS and pDOS for NpCuOP. $E_F = 0$ eV.

Calculation of formal oxidation states using the Bader charges gives unreasonable formal oxidation states of approximately An^{2+} and $Cu^{0.2+}$. Summing the calculated charges over the AnO and CuP layers is more informative. Two formal oxidation-state models An^{4+}/Cu^{1+} and An^{3+}/Cu^{2+} are supplied in Table 6. The sum of charges within the AnO layers for both compounds approaches the model for An^{3+}/Cu^{2+} with only an extra 0.15 e^- for UO and 0.23 e^- for NpO. Previous use of this method for LaFeOP determined a difference between the model and Bader charges of 0.36 e^- extra in the LaO layer that was attributed to La−P covalent interactions.[55] The relationship between the magnitude of the charge difference and the degree of covalency in an An−P bond is unclear, but the covalency of Np−P seems to be intermediate between La−P and U−P.

Discussion

Figure 11 displays the basic structures of the family of actinides that includes the current compounds as well as those of the parent and other related compounds. Previous discussions of this family of compounds have centered around division of a structure into different building blocks stacked in the *c*-direction.[3,34,78] In all of the related tetragonal compounds, the An atoms sit at C_{4v} centers of symmetry with eight anions in the first coordination sphere forming a square antiprism (Figure 11). For AnT_2 and AnPS compounds, there is an additional ninth capping anion interaction not retained in AnOS or any of the Cu-filled structures, but it has been omitted from the figure for the sake of clarity.

In all the compounds, the actinide square antiprisms face share in the *ab*-plane generating short An−An distances discussed above and listed in Table 7 as J_1. These interatomic distances are important to the electronic and magnetic properties and are exceedingly close to the Hill limit for U of 3.4 Å for direct 5f orbital overlap.[79] However, the differences in the properties of these compounds must be related to some additional structural difference in the second or third An coordination sphere. The stacking of the square antiprisms along the *c*-axis in UP_2, AnTQ, AnOS, AnCuOP, and the UCuOP-like U position of $U_2Cu_2OP_3$ is edge sharing that we designate as a Type I interaction. In $UCuP_2$ and the second U position of $U_2Cu_2OP_3$, this interaction is face sharing and designated here as Type II. Even though a clear crystal-field splitting model, such as that used in d-element chemistry, cannot easily be drawn for the f-orbitals in C_{4v} symmetry, the face-sharing interaction along the 4-fold major axis that is present only in the Type II compounds should lead to enhanced overlap of the $5f_{z^3}$ orbital. Because these longer An−An interactions have an effect on the properties of these compounds, they have been listed in Table 7 as J_2 and J_3, where J_2 is the edge- or face-sharing interaction and J_3 is the interaction across the empty tetrahedral holes or the Cu-layer.

The compounds UP_2, UOS, NpOS, and $U_2Cu_2OP_3$ all contain Type I interactions, as found in UCuOP. Those five compounds order antiferromagnetically at 203 K,[7] 55 K,[14] 4.2 K,[17,80,81] 146 K,[36] and 224 K, respectively. With the

(78) Albering, J. H.; Jeitschko, W. *Z. Naturforsch. B: Anorg. Chem. Org. Chem* **1996**, *51*, 257–262.

(79) Hill, H. H. In *Plutonium 1970 and Other Actinides*; Miner, W. N., Ed.; The Metallurgical Society of the American Institute of Mining, Metallurgical, and Petroleum Engineers, Inc.: New York, NY, 1970; Vol. *17*, pp 2−19.

(80) Thévenin, T.; Jové, J.; Pagès, M. *Mater. Res. Bull.* **1985**, *20*, 723–730.

(81) Collard, J. M.; Blaise, A.; Bogé, M.; Bonnisseau, D.; Burlet, P.; Fournier, J. M.; Larroque, J.; Beauvy, M. *J. Less-Common Met.* **1986**, *121*, 313–318.

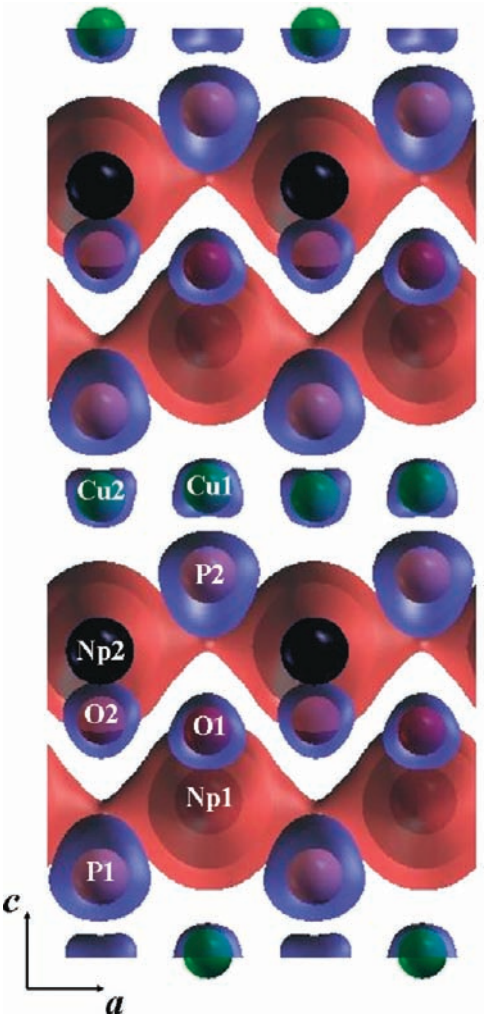

Figure 10. Isosurface plot of the magnetization distribution for NpCuOP with an isovalue of 0.01. An eight unit cells supercell ($2a \times 2b \times 2c$) is shown. The view is down [010]. In the figure, α-magnetization density (red) and β-magnetization density (blue) are plotted along with Np (black), Cu (green), O (red), and P (pink).

nomenclature devised earlier,[4] the stacking sequence of ferromagnetically aligned actinide layers along the *c*-axis may be described as AFII (+ − − +) in UP_2,[7] AFIII (+ + − −) in UOS,[14] and AFI (+ − + −) in UCuOP. More complex AF ordering is found in $U_2Cu_2OP_3$ (Type I and II), but between Type I U layers the ordering is AF.[82] The magnetic structure of NpOS remains unknown but is assumed to be that of NpOSe, AFI.[17] In these compounds J_1 is ferromagnetic whereas the shorter of J_2 and J_3 is antiferromagnetic (Table 7). The ratio J_3/J_2 is much closer to unity in UP_2 and UOS than it is in UCuOP. This may be why the magnetic unit cells of UP_2 and UOS are $a \times b \times 2c$, but the crystallographic and magnetic cells coincide in UCuOP.

In UP_2 and UOS, the formation of a larger magnetic unit cell decreases the size of the Brillouin zone thereby changing the shape of the Fermi surface and directly affecting the electronic properties.[83] The magnetic-resistive interaction is clearest in UP_2 where the resistivity within the ferromagnetic basal plane ($\rho_\perp$) increases with temperature until T_N and then

(82) Burlet, P.; Troc, R.; Kaczorowski, D.; Noël, H.; Rossat-Mignod, J. *J. Magn. Magn. Mater.* **1994**, *130*, 237–241.
(83) Meaden, G. T. *Contemp. Phys.* **1971**, *12*, 313–337.

Table 6. Calculated Total Atomic and Layer Charges (e^-) for UCuOP and NpCuOP[a]

species	R_{WS} charge[b]	Bader charge	purely ionic An^{4+}/Cu^{1+}	purely ionic An^{3+}/Cu^{2+}
U	9.69	11.94	10	11
Cu	9.33	10.83	10	9
P	7.68	6.01	8	8
O	7.67	7.22	8	8
UO	17.35	19.15	18	19
CuP	17.01	16.85	18	17
Np	11.52	13.04	11	12
Cu	8.92	10.82	10	9
P	7.30	5.95	8	8
O	7.96	7.18	8	8
NpO	19.48	20.23	19	20
CuP	16.22	16.77	18	17

[a] Maximum total charge is 36 e^- for UCuOP and 37 e^- for NpCuOP. [b] R_{ws} values (Å): UCuOP: U, 1.5 ; Cu, 1.1; O, 1.5; P, 1.8; NpCuOP: Np, 1.31; Cu, 1.25; O, 1.5; P, 1.9.

becomes nearly temperature independent.[9] Conversely, the longitudinal resistivity ($\rho_\parallel$) (AF direction) displays a characteristic "hump backed" trend, increasing with temperature and reaching a maximum at approximately 120 K before decreasing until T_N (203 K).[9] Even though UOS displays insulating resistivity in the high-temperature paramagnetic region,[15,16] its larger magnetic unit cell could lead to similar trends in the ordered low-temperature regions. Longitudinal resistivity of $U_2Cu_2OP_3$ also shows a similar "hump backed" increase that is centered around 43 K and levels off at approximately 200 K.[36] This is consistent with an antiferromagnetic structure similar to that of UP_2[6,7] but with a larger number of F ordered layers along the *c*-direction.

Of the two compounds with Type II interactions, namely, $UCuP_2$ and $U_2Cu_2OP_3$, the former orders ferromagnetically at 74.5 K and displays typical ferromagnetic temperature-dependent resistivity.[10−12] Complex antiferromagnetic ordering in the latter compound leads to anisotropy in its susceptibility and to a low-temperature increase at ∼80 K.[36,82] Temperature-dependent resistivity also fits well with the low-temperature "hump-back" in the longitudinal resistivity and with metallic conductivity in the ordered region with the characteristic "knee" at the Néel point for the basal-plane resistivity.[71] Neutron diffraction experiments on $U_2Cu_2OP_3$ show the Type I interactions are AF, whereas the Type II are F.[82] The stacking of two Type I and two Type II layers leads to + + − − − − + + stacking of the U layers. The AF interactions are across the O layer and between Type I U layers, whereas the Type I U layer orders F with its closest Type II U layer. The antiferromagnetically ordered Type I U1 ions order with 2.2 μ_B moments but the ferromagnetically ordered Type II U2 ions order with 1.1 μ_B moments.[82] Even though this change in magnitude might suggest mixed valence U, the compound charge balances with all tetravalent U and the moments correspond well to those found for Type I interactions here for UCuOP, 2.42 μ_B, and for Type II interactions in $UCuP_2$, 0.98 μ_B.[10]

The properties of UCuOP determined in this work fit well into the framework described above for this family of compounds. Because the U sheets in UCuOP order ferromagnetically, it is not surprising that resistivity within this layer mirrors that of UP_2 and $UCuP_2$. Even though UOS is a semiconductor in the paramagnetic region, resistivity measurements in the ordered region might be revealing because

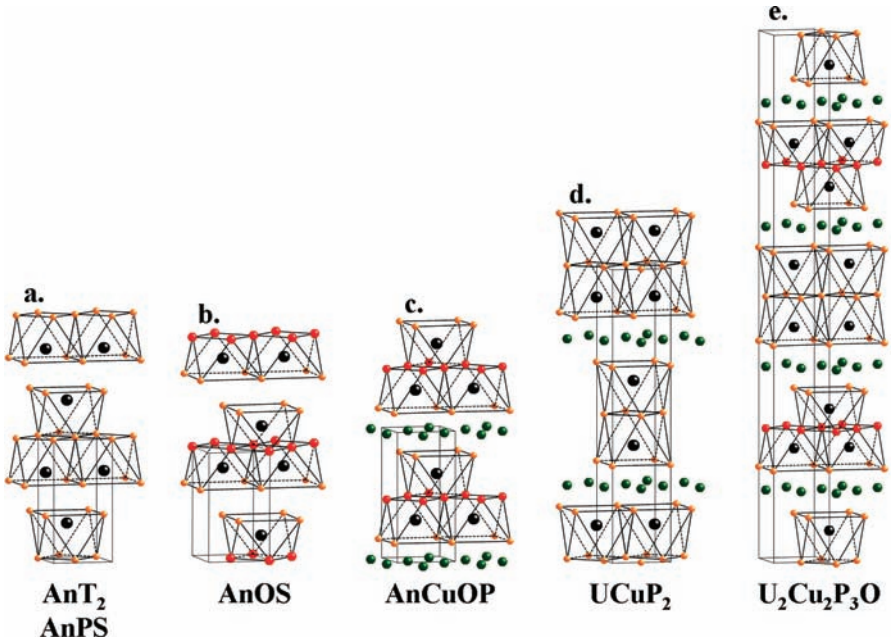

Figure 11. Structures of (a) AnT_2 and AnPS (An = U, Np; T = pnictide); (b) AnOS (An = U, Np); (c) AnCuOP (An = U, Np); (d) $UCuP_2$; and (e) $U_2Cu_2OP_3$.

Table 7. Properties of Related Compounds[a]

species	ordering type[b]	$T_{C,N}$ (K) from χ vs T	$\rho_\perp$	$\rho_\parallel$	$T_{C,N}$ (K) from ρ vs T	J_1 (Å)	J_2 (Å)	J_3 (Å)
UP_2	AFII	203	increase to T_N	hump back	203	3.318(5) (F)	5.115(3) (F)	4.351(2) (AF)
UAs_2	AFII	283	increase to T_N		274	3.962(1)	5.347(1)	4.5444(8)
$NpAs_2$	F	18	peak at T_C		17.8			
	AF[c]	52	small blip		48	3.930(5)	5.351(3)	4.519(2)
UOS	AFIII	55				3.8436(2) (F)	3.8284(2) (AF)	4.8339(3) (F)
NpOS	AFI	4.2				3.825(2) (F)	3.79(4) (AF)	4.82(5) (AF)
$UCuP_2$	F	74.5	increase to T_C		74	3.803(1) (F)	4.094(8) (F)	5.826(7) (F)
UCuOP	AFI	222	hump back		187	3.7817(4)(F)	3.8128(7)(AF)	6.122(1)(AF)
NpCuOP	F[d]		section III.C		90	3.7731(4)(F)[d]	3.7813(6)(F)[d]	6.1211(8)(F)[d]
$U_2Cu_2OP_3$[e]	AF	146		hump back	134			
U1	AF					3.803(1)	3.8205(9)	5.965(1)
U2	F					3.803(1)	4.116(1)	5.965(1)

[a] As a general reference see *The Chemistry of the Actinide and Transactinide Elements*; Morss, L. R., Edelstein, N. M., Fuger, J., Eds., Springer 2010. [b] AFI (+ − + −), AFII (+ − − +), and AFIII (+ + − −) as defined in ref 4. [c] $NpAs_2$ orders AF with incommensurate modulation propagating along [100]. [d] Current theoretical results. [e] The U1 positions are type I; the U2 positions are type II.

the structure and interatomic distances are closer to those of UCuOP but it orders magnetically in the longer range AFIII manner. The semimetallic resistivity of UCuOP also fits well with the present LSDA + GGA + SOC calculations that find the DOS at $E_F \neq 0$ to be asymmetric with respect to electron spin. Even though addition of an on-site Coulomb correction could shift the location of E_F and split the 5f orbitals, this should not change the semimetallic conduction within each ferromagnetic U sheet. Comparative electronic structure calculations on other antiferromagnetic compounds of this family are needed.

Owing to the very limited number of known Np/P compounds and minimal knowledge of their properties, structure−property comparisons cannot be made. Nonetheless, the intriguing properties of the known compounds, including those reported here, strongly suggest that the electronic structures of isostructural Np and U compounds are very different. The trend in the basal-plane resistivity found here for NpCuOP suggests antiferromagnetic ordering, but it more closely resembles the longitudinal resistivity of the antiferromagnetic U compounds.[9,71] Even though the calculated DOS for the lowest-energy ferromagnetically aligned single unit cell of NpCuOP resembles that of UCuOP, the increased Cu moment in NpCuOP compared to that in UCuOP and the charge distribution within the AnO layers of NpCuOP suggest an intermediate nature of NpCuOP between that of LaFeOP and UCuOP. The supercell calculations suggest increased complexity for the magnetic alignment of Np atoms in NpCuOP. As the number of multinary compounds of Np increases, our understanding of this intermediate actinide and the entire actinide series will also increase.

Acknowledgment. We are grateful for the support of Dr. L. Soderholm and Dr. S. Skanthakumar of the Actinide Facility of Argonne National Laboratory where we performed the neptunium synthetic work. We are also grateful to Dr. Geng Bang Jin at Northwestern University and Argonne National Laboratory and George Oh at Northwestern University for their help. The research at Northwestern University was kindly supported by the U.S. Department of Energy, Basic Energy Sciences,

Chemical Sciences, Biosciences, and Geosciences Division and Division of Materials Sciences and Engineering Grant ER-15522. D.M.W. acknowledges partial support from the MRSEC program of the National Science Foundation (DMR-0520513). Use was made of the Materials Research Science and Engineering Center, Magnet and Low Temperature Facility supported by the National Science Foundation (DMR-0520513).

Supporting Information Available: The crystallographic files in CIF format for UCuOP and NpCuOP as well as the neutron diffraction data for UCuOP. This material is available free of charge via the Internet at http://pubs.acs.org.